CHAPTER 4

Results

For the first phase results, the DIR accuracy on MVCT images by eight DIR methods were quantified in phantom and NPC cases for known and unknown offset investigation. The correlation between the DIR accuracy on kVCT and MVCT images were explored. The best three DIR methods were selected to use in the second phase. As regards the second phase for accumulated dose evaluation, the ROIs volume variations were considered and the accuracy of weekly registration was analyzed. The dose summation by used the Planned adaptive software and DIRART software were compared. The difference between the accumulated dose and the initial planned dose were analyzed, then evaluated the impact of three DIR methods for estimated the dose accumulation in terms of uncertainty values.

4.1 Phase I: DIR accuracy on MVCT images quantification

4.1.1 Known offset investigation: Phantom studies

The in-house acrylic phantom in various sizes and shapes inserted in cubic phantom were used to simulate the rigid volume changes of the target and OAR with its known offset values. The tissue equivalent materials in the bent, curved, and pressed shapes were inserted in the cubic phantom to simulate the non-rigid volume changes.

1) Intensity-based criterion:

Figure 4.1 shows the intensity difference between the original images and deformed images before and after DIR by the eight methods in phantom with bent shape. The forward mapping showed a lower intensity difference

after DIR as in methods no. 2, 4, 6, and 8. However, the symmetric transformation as in methods no.5 and 7 also showed a lower intensity difference for backward mapping.

Regarding the validation in the intensity-based criterion, the values of the mean square different (MSD), correlation coefficient (CC) and normalized mutual information (NMI) were used to ensure image matching quality. MSD will be zero when the images are correctly aligned and will increase with registration error, CC can take values between −1 and +1, where +1 represents the maximum correlation between images, NMI can range between 0 and 2, and values of NMI > 1 typically represent a good match between images. The Figure 4.2 showed the validation in terms of the intensity-based criterion with MSD, CC and NMI values for rigid and non-rigid volume changes.

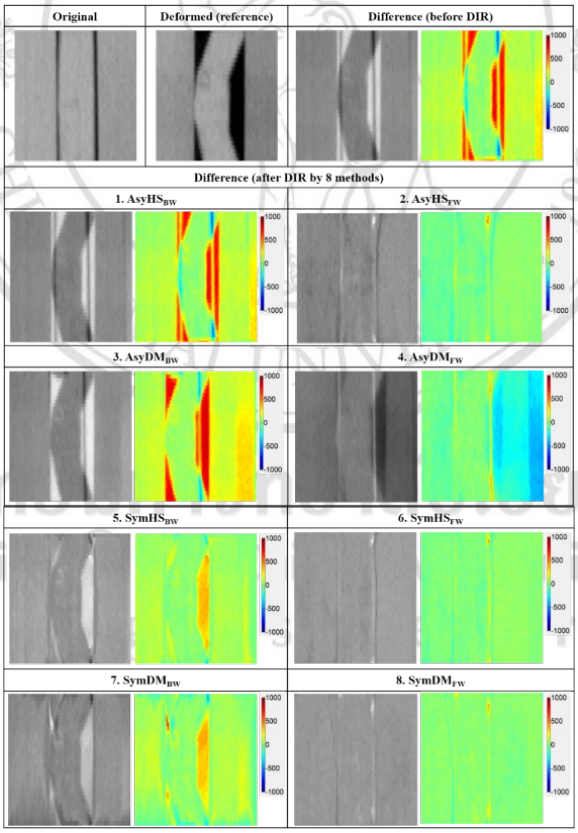

Figure 4.1 Coronal plane intensity different images between the original images and deformed images before and after DIR by the eight methods of phantom with bent shape.

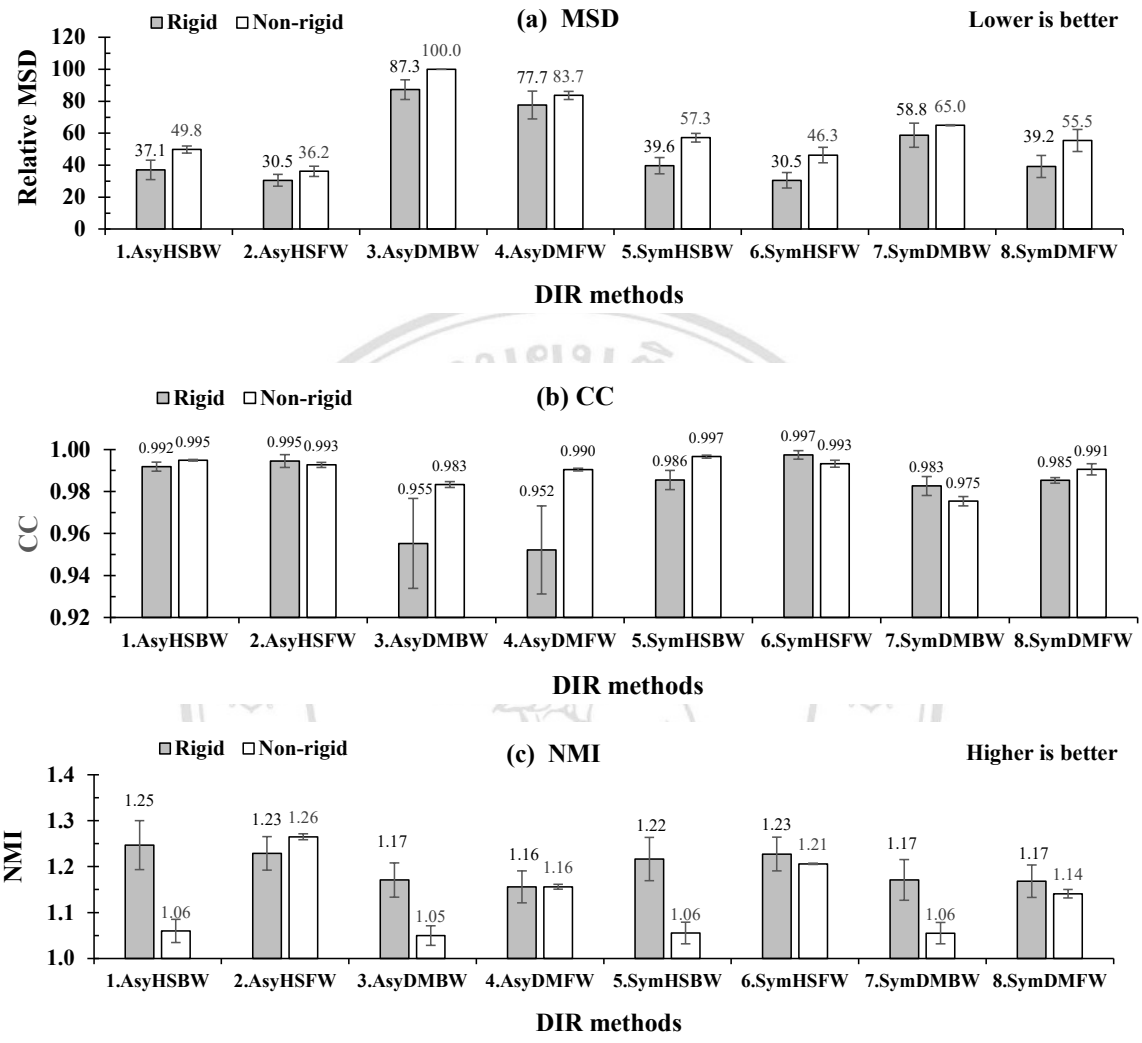

Figure 4.2 The validation for known offset investigation in terms of the intensity-based criterion with (a) the mean square different, *MSD*, (b) the correlation coefficient, *CC* and (c) the normalized mutual information, *NMI*

Regarding the rigid volume changes, there were concordance of the results with MSD, CC and NMI. The Horn and Schunck optical flow showed the better performance than the Demons in both transformations and mapping directions as showed in the methods number 1, 2, 5 and 6 (1 = $AsyHS_{BW}$, 2 = $AsyHS_{FW}$, 5 = $SymHS_{BW}$ and 6 = $SymHS_{FW}$) in Figure 4.2. The $AsyHS_{FW}$ (no.2) demonstrated the best agreement with the lowest mean values of relative MSD = 30.5 ± 12.3 and the highest mean values of CC = 0.997 ± 0.007 was detected in the $SymHS_{FW}$ (no.6). However, the $AsyHS_{BW}$ (no.1)

showed the best performance with a highest mean value of NMI = 1.25 ± 0.177.

As regards the non-rigid volume changes, there were also concordance of the results with MSD and CC. The Horn and Schunck optical flow still showed the better performance than the Demons in the methods number 1, 2, 5 and 6. The best performance was the $AsyHS_{FW}$ (no.2) with a mean relative MSD = 36.2 ± 12.3 and the $SymHS_{BW}$ (no.5) showed the best with a mean value of CC = 0.997 ± 0.002. However, the $AsyDM_{FW}$ (no.4) showed increasing in NMI with the mean value = 1.16 ± 0.018 and the $AsyHS_{FW}$ (no.2) showed the best performance with mean value of NMI = 1.26 ± 0.021 as in Figure 4.2(c).

2) Volume-based criterion:

Regarding the validation in the volume-based criterion, the overlapping volume of the structure which is created by the radiation oncologist and the DIRART deformed were demonstrated in Figure 4.3. The most common overlap metric is the Dice Similarity Coefficient (DSC). If the images have no overlap, then the DSC is 0, and as the contours become identical, the DSC approaches a value close to 1. The DSC value greater than 0.7 is typically selected to indicate good segmentation performance (Kristy et al., 2013).

(a)

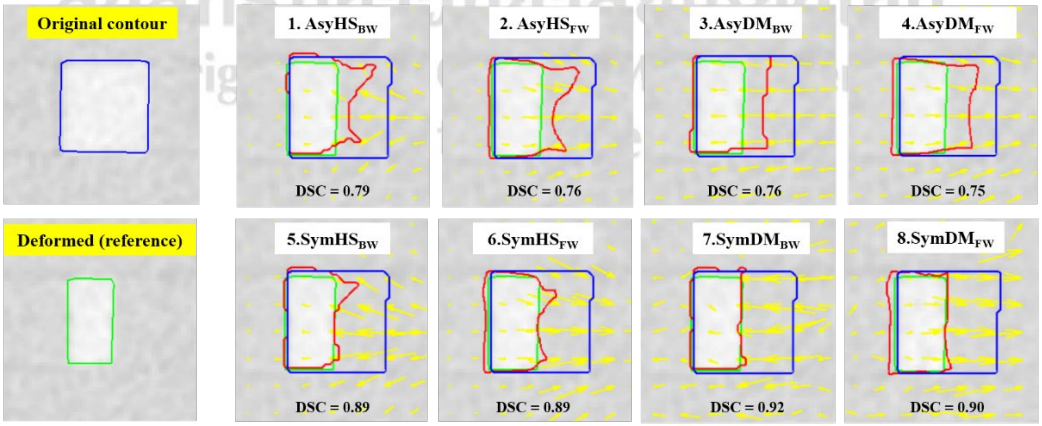

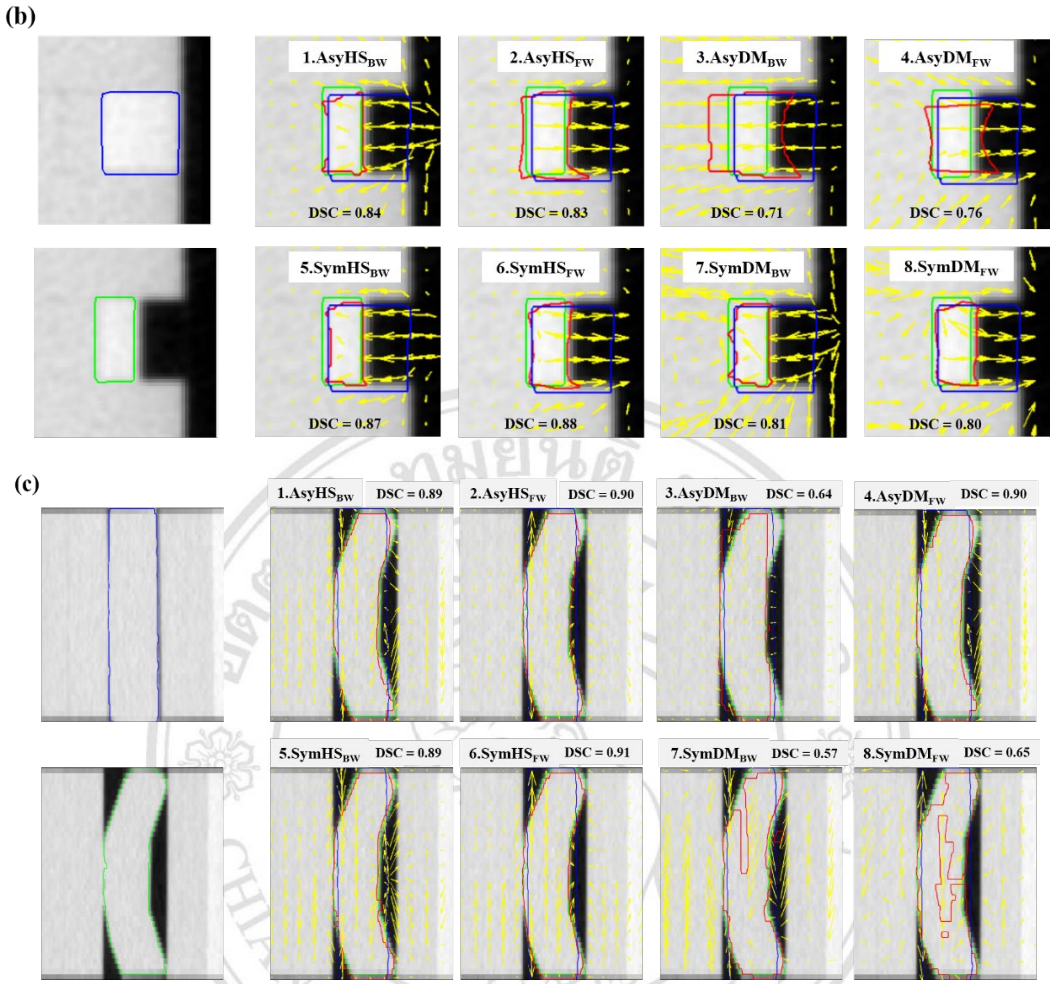

Figure 4.3 The deformation vector field (yellow arrows) used to identify the motion from the original contours (blue line), which is compared between the reference contours (green line), and the automatic contours (red line) with the mean value of DSC by eight DIR methods for rigid changes (a) no.1 and (b) no.8 and non-rigid volume changes (c) no.10.

The results of volume-based criterion in terms of DSC value were concordant with the intensity-based analysis. The DIR methods number 1, 2, 5 and 6 (1 = AsyHS$_{BW}$, 2 = AsyHS$_{FW}$, 5 = SymHS$_{BW}$ and 6 = SymHS$_{FW}$) also showed better performance in both rigid and non-rigid volume changes than the remainder methods as in Figure 4.3. The SymHS$_{FW}$ (no.6) demonstrated the best performance with a mean value of DSC = 0.899 ± 0.03 for rigid changes and 0.913 ± 0.01 for non-rigid volume changes. However, for the Demons algorithm, the mean value of DSC for AsyDM$_{FW}$ (no.4) method was

found to be significantly increased in the non-rigid volume changes as in Figure 4.4.

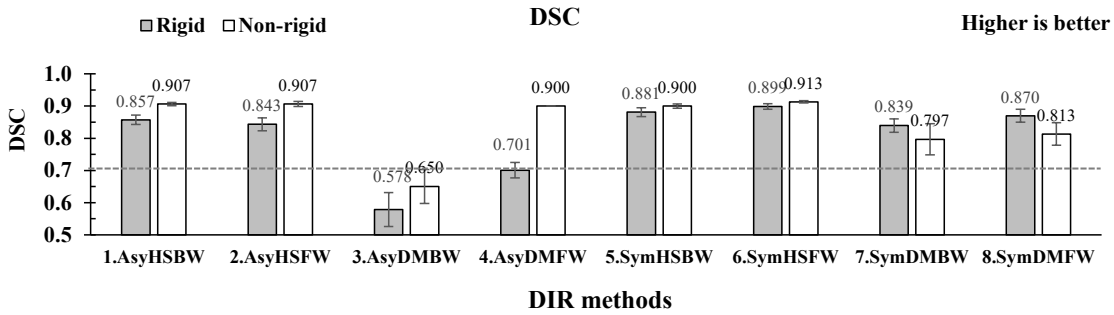

Figure 4.4 The DSC value of eight DIR methods for known offset investigation.

3) Deformation field analysis:

As regards the deformation field analysis, the inverse consistency error (ICE) and the Jacobian analysis were used to ensure that the transformations were physically plausible. The optimal transformation was found when the ICE minimized the distance error. The Jacobian matrix describes how the transformation changes in each of the three directions. The Jacobian $J_T(x) = 1$ if the volume at x remains the same after the transformation, $J_T(x) > 1$ if there is volume expansion and $J_T(x) < 1$ if there is volume shrinkage. The mean of ICE and Jacobian analysis are shown in Table 4.1.

Table 4.1 The mean of inverse consistency error (ICE) and Jacobian analysis of rigid volume changes in eight DIR methods.

		ICE (mm)		Jacobian	
No.	DIR methods	Rigid	Non-rigid	Rigid	Non-rigid
1	$AsyHS_{BW}$	0.1735	0.1313	0.9726	1.0043
2	$AsyHS_{FW}$	0.0647	0.0361	1.0102	1.0121
3	$AsyDM_{BW}$	0.0658	0.5471	0.9871	0.9922
4	$AsyDM_{FW}$	0.0248	0.0456	1.0070	1.0046
5	$SymHS_{BW}$	0.3098	0.5412	0.9737	0.9676
6	$SymHS_{FW}$	0.1557	0.0504	1.0262	1.0310
7	$SymDM_{BW}$	1.4286	2.8133	0.9360	0.9987
8	$SymDM_{FW}$	0.3167	0.6865	0.9924	1.0121

Regarding the ICE analysis, the asymmetric showed better performance than the symmetric transformation in both rigid and non-rigid volume changes. The $AsyDM_{FW}$ (no.4) demonstrates the best agreement at mean values of ICE = 0.025 ± 0.05 mm. for rigid changes and the $AsyHS_{FW}$ (no.2) showed the best performance at mean values of ICE = 0.036 ± 0.02 mm. for non-rigid changes.

However, the results of the Jacobian analysis showed the better with Demons than Horn and Schunck optical flow. The $AsyDM_{FW}$ (no.4) methods also showed better performance, with mean values of Jacobian = 1.0070 ± 0.01 for rigid and the $SymDM_{BW}$ (no.7) showed the best performance at mean values of Jacobian = 0.9987 ± 0.02 for non-rigid volume changes.

4.1.2 Unknown offset investigation: Clinical studies

The prospective data from five nasopharyngeal carcinoma patients who were treated using a helical tomotherapy treatment machine were used. The 1st DAY MVCT images were acquired on the helical tomotherapy unit as the source images on the same day of planning kVCT image acquisitions, and the 20th fraction MVCT images were also acquired as the target images for registration.

1) Intensity-based criterion:

Figure 4.5 shows the intensity difference images between the original images and deformed images before and after DIR by the eight methods in NPC patient no.1. The Horn and Schunck optical flow showed slightly lower intensity difference after DIR as in methods no. 1, 2, 5 and 6.

Regarding for assessed in clinical cases, there were concordance of the results with MSD, CC and NMI. The Horn and Schunck optical flow showed better performance than the Demons in both transformations and mapping directions as shown in the methods number 1, 2, 5 and 6 (1 = $AsyHS_{BW}$, 2 = $AsyHS_{FW}$, 5 = $SymHS_{BW}$ and 6 = $SymHS_{FW}$) in Figure 4.6. The $AsyHS_{FW}$ (no.2) demonstrated the best agreement with the lowest mean values of relative MSD = 52.8 ± 8.0 and the highest mean values of CC = 0.983 ± 0.016.

Moreover, the $AsyHS_{FW}$ (no.2) also showed the best performance with the highest mean value of NMI = 1.214 ± 0.12.

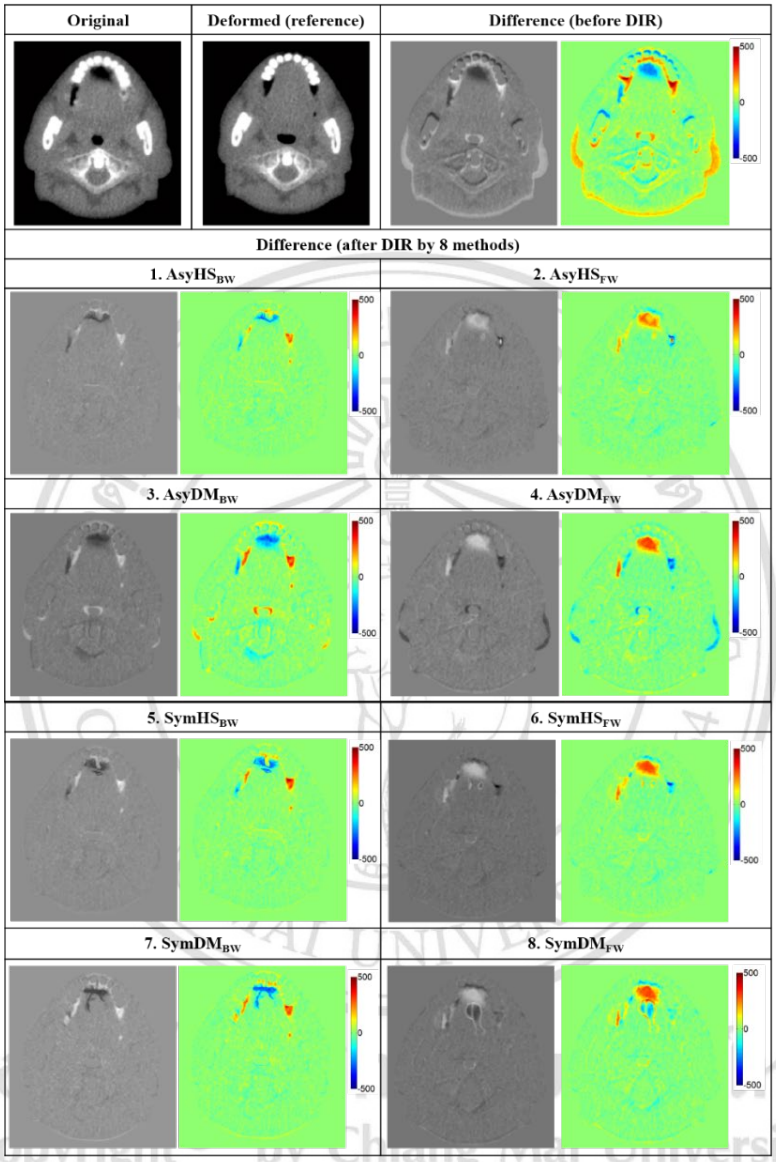

Figure 4.5 Transverse plane intensity difference images between the original images and deformed images before and after DIR by eight methods of NPC patient no.1.

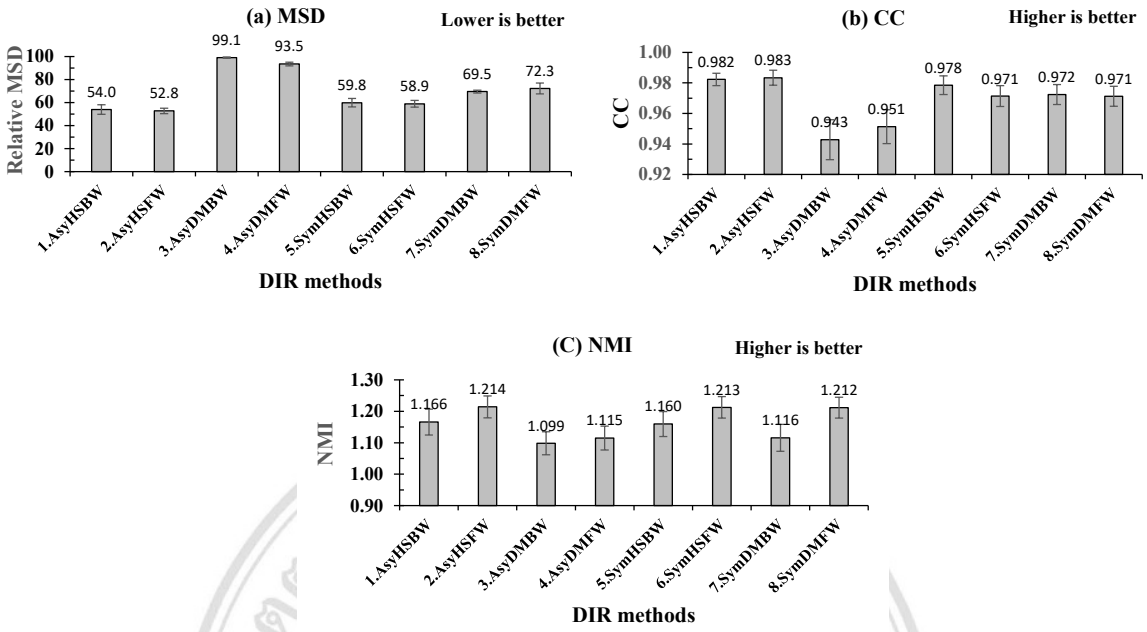

Figure 4.6 The validation for unknown offset investigation in terms of the intensity-based criterion with (a) the mean square different, *MSD*, (b) the correlation coefficient, *CC* and (c) the normalized mutual information, *NMI*

2) Volume-based criterion:

The overlapping volume of the structure which is created by the radiation oncologist and the DIRART deformed were assessed. The satisfactory volume matching should be 70% (DSC 0.7) or more for adaptive radiotherapy application (Zimring *et al*., 2005). The structure, including the GTV, CTV, the bilateral parotid glands, and spinal cord were used to observe the automatic deformed structure created by DIRART software in eight DIR methods was demonstrated in Figure 4.7 for the non-rigid organs (GTV, right parotid gland) and rigid organ changes (spinal cord).

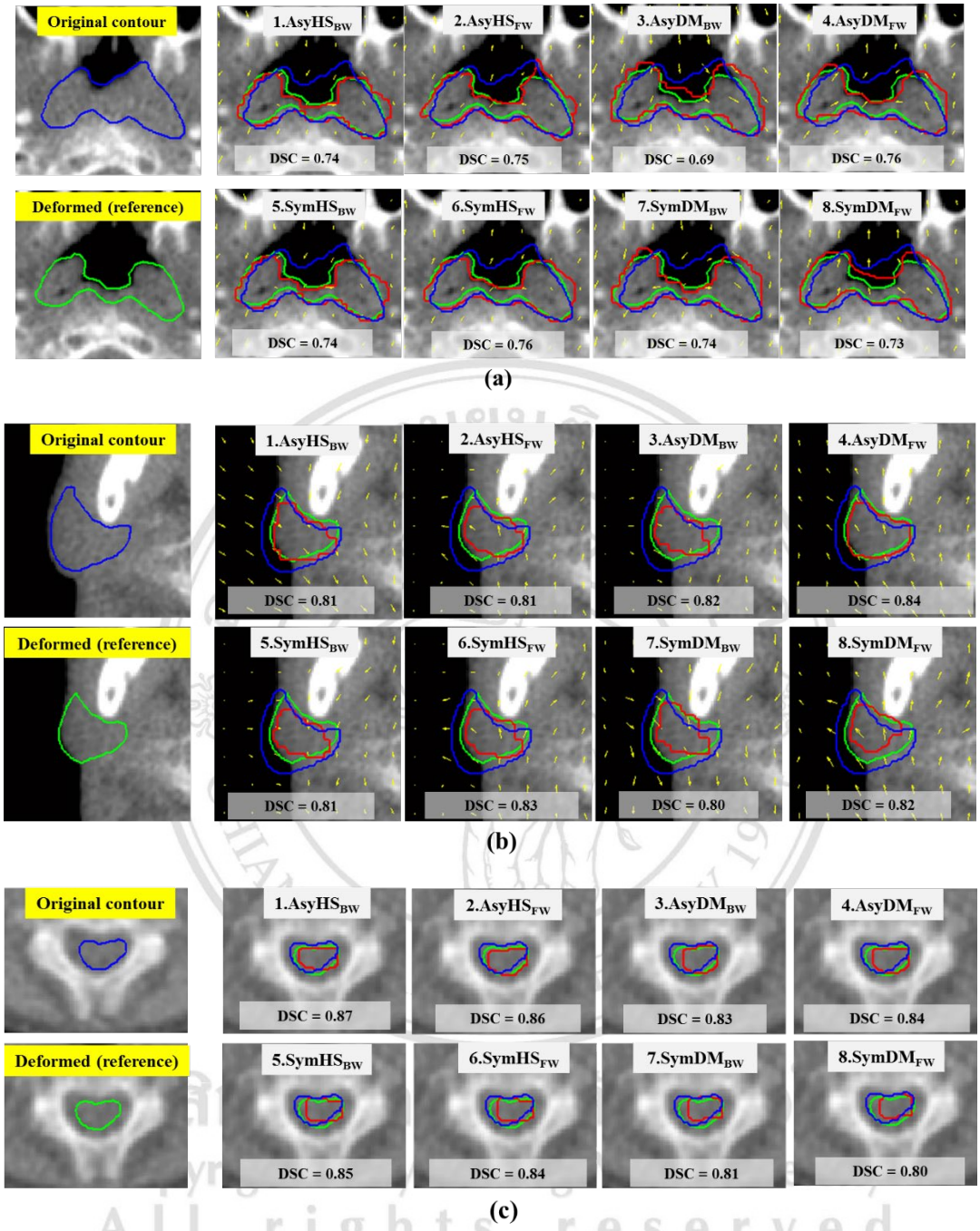

Figure 4.7 The deformation vector field (yellow arrows) used to identify the motion from the original contours (blue line), which is compared between the reference contours (green line), and the automatic contours (red line) with the mean value of DSC by eight DIR methods for (a) gross tumor volume, GTV (b) right parotid gland and (c) spinal cord.

The volume-based criterion in terms of DSC were also concordant with the intensity-based analysis. The DIR methods number 1, 2, 5 and 6 (1 = $AsyHS_{BW}$, 2 = $AsyHS_{FW}$, 5 = $SymHS_{BW}$ and 6 = $SymHS_{FW}$) also showed better performance in both rigid and non-rigid organs than other methods as in Figure 4.8. However, for the $AsyDM_{FW}$ (no.4), the mean value of DSC was found to be significantly increased in the non-rigid organs and reached the best performance with DSC = 0.812 ± 0.07, as demonstrated in Figure 4.8. The $AsyHS_{FW}$ (no.2) demonstrated the best performance with a mean value of DSC = 0.806 ± 0.05 for spinal cord (rigid organ).

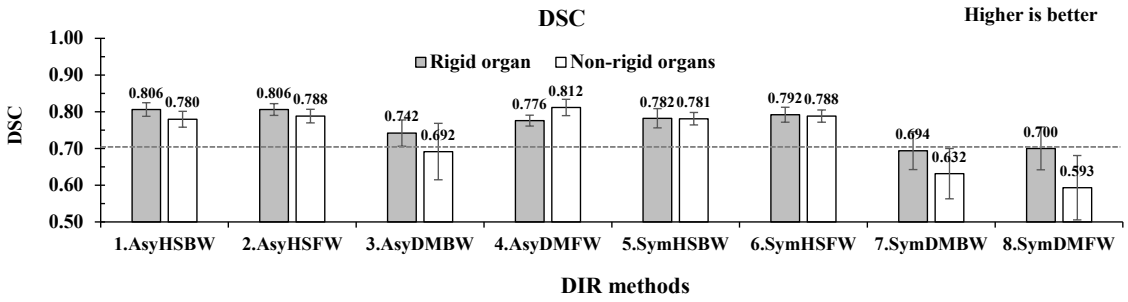

Figure 4.8 The DSC value of eight DIR methods for unknown offset investigation in rigid and non-rigid organs.

3) Deformation field analysis:

As regards the deformation field analysis, the optimal transformation was found when the ICE minimized the distance error. The Jacobian matrix describes how the transformation changes in each of the three directions. The mean of ICE and Jacobian analysis for NPC images are shown in Table 4.2.

Table 4.2 The mean of inverse consistency error (ICE) and Jacobian analysis of NPC images by eight DIR methods.

No.	DIR methods	ICE (mm)	Jacobian
1	$AsyHS_{BW}$	0.0885	1.0146
2	$AsyHS_{FW}$	0.0621	1.0452
3	$AsyDM_{BW}$	0.1687	0.9261
4	$AsyDM_{FW}$	0.0411	0.9885
5	$SymHS_{BW}$	0.4239	0.9626
6	$SymHS_{FW}$	0.1766	1.0247
7	$SymDM_{BW}$	1.3583	0.8973
8	$SymDM_{FW}$	0.9983	1.0019

Regarding the ICE analysis in NPC case, there were concordant with phantom analysis. The asymmetric showed better performance than the symmetric transformation in both DIR algorithms. The $AsyDM_{FW}$ (no.4) demonstrated the best agreement at mean values of ICE = 0.041 ± 0.05 mm. Moreover, there were concordance with phantom studies for the results of the Jacobian analysis, the Demons showed better performance than Horn and Schunck optical flow. The $SymDM_{FW}$ (no.8) methods showed good performance with mean values of Jacobian = 1.0019 ± 0.17 for NPC patient images.

4.1.3 Correlation between DIR accuracy on kVCT and MVCT images

Regarding the correlation between DIR accuracy on kVCT and MVCT images, the validation in terms of intensity-based, volume-based and deformation analysis on both kVCT and MVCT images were compared, when using different deformation methods assessed in known offset (phantoms) and unknown offset (NPC patients).

1) Intensity-based criterion

Regarding the comparison with the intensity-based criterion, the values of the CC and NMI were consistent between the DIR on the kVCT and the MVCT images for both phantom and NPC cases. Figure 4.9 demonstrates the phantom with (a) the rigid and (b) the non-rigid volume changes, the CC

analysis of the DIR of the kVCT images revealed that the kVCT images were not significantly better than the MVCT images, with p-value = 0.5345 and 0.1624, respectively. As for the NPC cases, it was found that there was no significant difference between the DIR on the kVCT and the MVCT images, with p-value = 0.3986, as shown in Figure 4.9 (c).

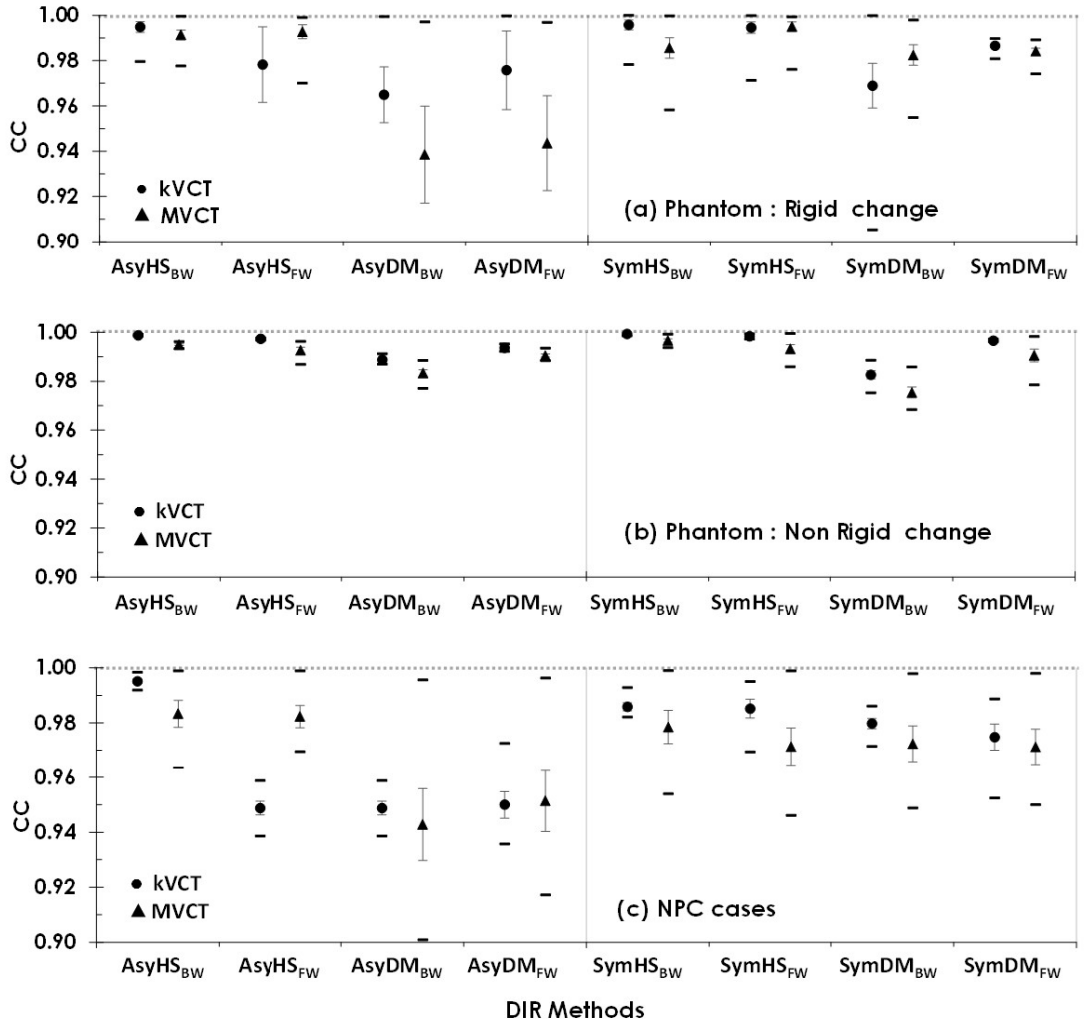

Figure 4.9 Comparison of the correlation coefficient (cc) in kVCT and MVCT deformable image registration. The results of the mean, standard error (vertical lines), and range (horizontal lines) given by eight deformable registration methods for (a) phantom with rigid volume changes, (b) phantom with non-rigid volume changes, and (c) NPC cases.

As regards the NMI analysis, DIR on the kVCT image was found to be significantly better than that on the MVCT image in phantom for rigid volume changes, as illustrated in Figure 4.10 (a), with p-value = 0.0011. However, there was no significant difference in NMI between the DIR on the kVCT and the MVCT images in phantom with non-rigid volume changes, as shown in Figure 4.10 (b), with p-value = 0.4762, and in NPC cases, as shown in Figure 4.10 (c), with p-value = 0.2165.

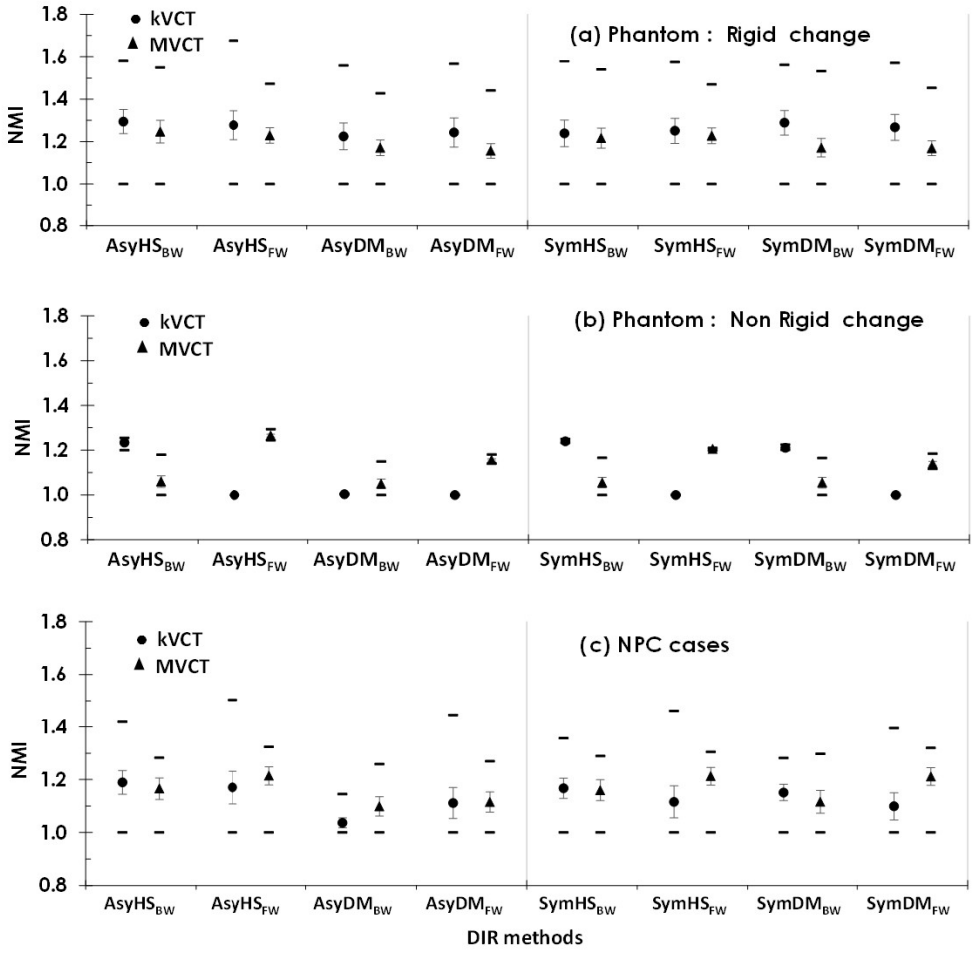

Figure 4.10 Comparison of normalized mutual information (NMI) in kVCT and MVCT deformable image registration. The results of the mean, standard error (vertical lines), and range (horizontal lines) given by eight deformable registration methods for (a) phantom with rigid volume changes, (b) phantom with non-rigid volume changes, and (c) NPC cases.

2) Volume-based criterion

The results of DIR accuracy in terms of DSC were consistent between kVCT and MVCT images for both phantom and NPC cases. Figure 4.11 demonstrates the phantom with rigid (a) and non-rigid (b) volume changes; the DSC values of DIR in the kVCT images were not significantly better than the DSC values of the MVCT images, with p-value = 0.8504 and 0.6741, respectively. The DSC values of NPC cases in the kVCT images, as illustrated in Figure 4.11(c), were found to be significantly better than the DSC values of NPC cases in the MVCT images, with p-value = 0.0006 for the rigid volume changes. However, for the non-rigid changes, the DSC values were not significantly different with p-value = 0.8722, as demonstrated in Figure 4.11(d).

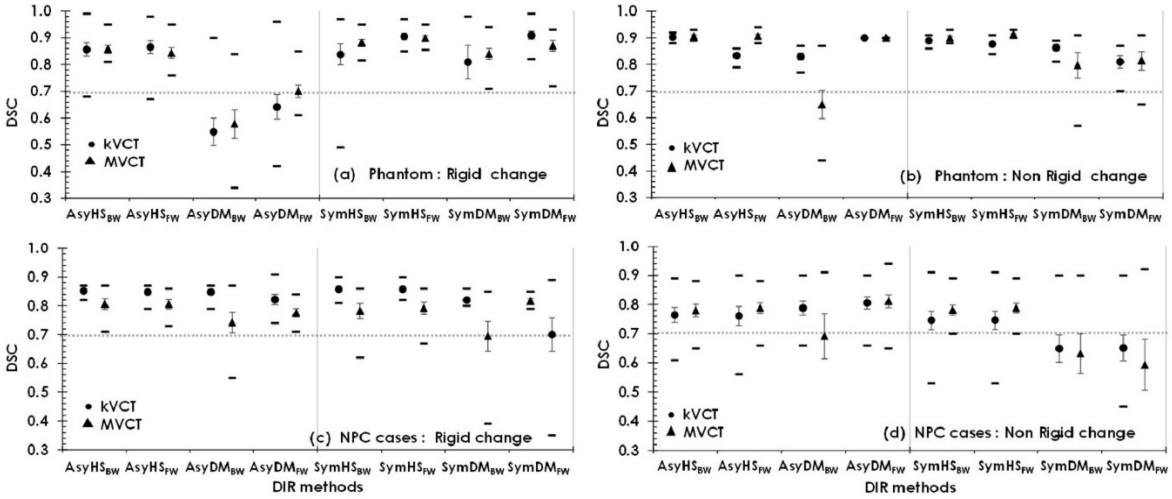

Figure 4.11 Comparison of the dice similarity coefficient (DSC) in kVCT and MVCT deformable image registration. The results of the mean, standard error (vertical lines), and range (horizontal lines) given by eight deformable registration methods for (a) phantom with rigid volume changes (b) phantom with non-rigid volume changes, (c) NPC cases with rigid volume changes, and (d) NPC cases with non-rigid volume changes in comparison of kVCT and MVCT images.

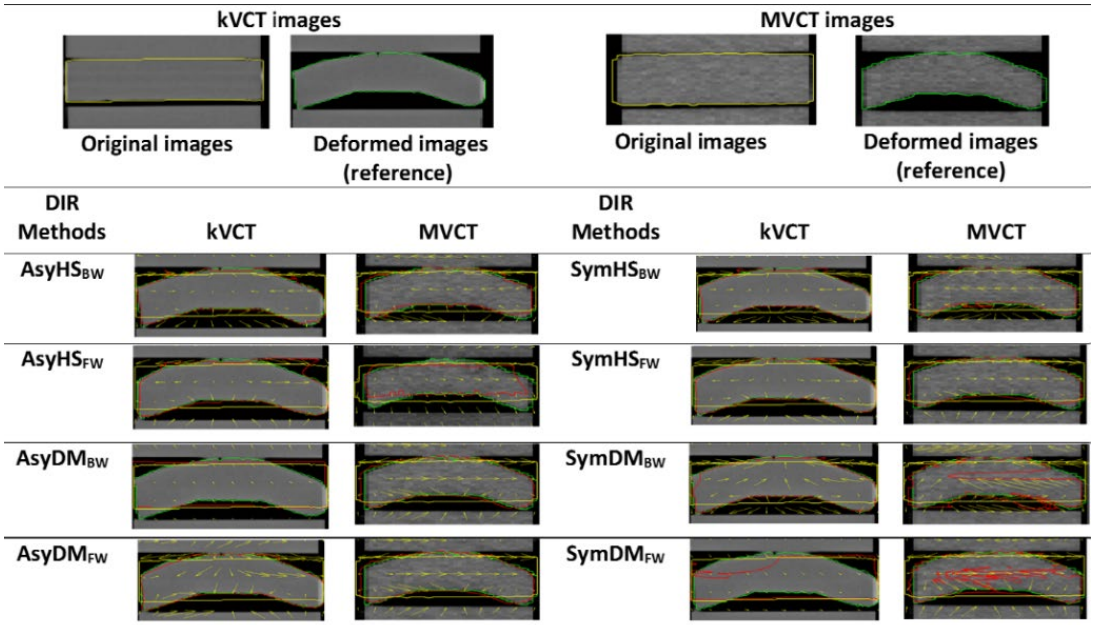

Figure 4.12 The DVF (yellow arrows) used to identify the motion, which is compared between kVCT and MVCT images from the original contours (yellow line), the reference contours (green line), and the automatic contours with eight DIR methods (red line) for phantom in bent shape.

Figure 4.12 illustrates the comparison of DIR between kVCT and MVCT images. Tissue equivalent materials in bent shapes were used to simulate the non-rigid volume changes. There was consistency between kVCT and MVCT images. The Horn and Schunck optical flow in both asymmetric and symmetric transformations showed better agreement of the deformed structure with the reference structure. However, the Demon in the asymmetric transformation with the forward method (AsyDM$_{FW}$) showed good agreement in both kVCT and MVCT images.

The comparison of DIR on the kVCT and MVCT images of the right parotid gland deformation of one NPC case is shown in Figure 4.13. The AsyDM$_{FW}$ method showed the best performance in the MVCT images. As for the kVCT images, the DIR methods slightly affected the accuracy of the kVCT images in this case.

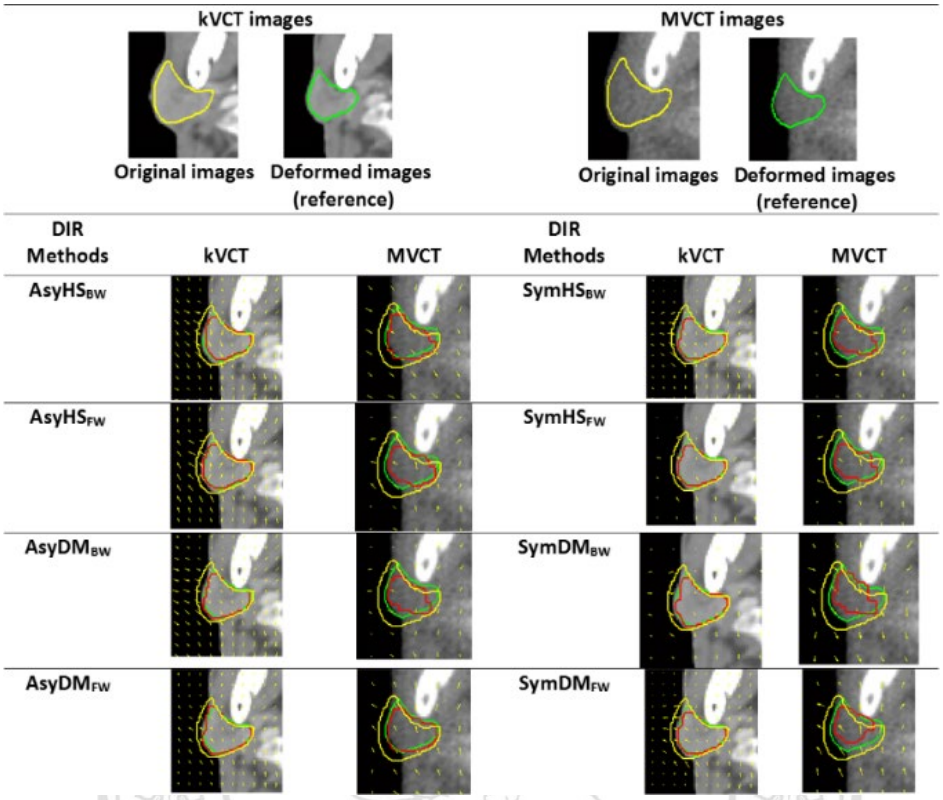

Figure 4.13 The DVF (yellow arrows) used to identify the motion, which is compared between kVCT and MVCT images from the original contours (yellow line), the reference contours (green line), and the automatic contours with eight DIR methods (red line) for the right parotid glands in one NPC patient.

3) Deformation field analysis

For the deformation field analysis, ICE was used to ensure that the forward and backward transformations were inverse-consistent. Table 4.3 demonstrates that the ICE values were not significantly different between DIR in the kVCT images and DIR in the MVCT images, with the p-value = 0.7847, 0.4387, and 0.0755 for phantom with rigid changes, phantom with non-rigid changes, and clinical cases, respectively.

Table 4.3 Inverse Consistency Error (ICE) comparison with different DIR methods between kVCT and MVCT images for phantom with both rigid and non-rigid changes and NPC cases.

DIR methods	Inverse Consistency Error (ICE)					
	Phantom (Rigid)		Phantom (Non rigid)		NPC cases	
	kV	MV	kV	MV	kV	MV
$AsyHS_{BW}$	0.1785	0.1735	0.0150	0.1313	0.0139	0.0885
$AsyHS_{FW}$	0.0339	0.0647	0.0212	0.0361	0.0181	0.0621
$AsyDM_{BW}$	0.0740	0.0658	0.0264	0.5471	0.0077	0.1687
$AsyDM_{FW}$	0.0062	0.0248	0.0421	0.0456	0.0041	0.0411
$SymHS_{BW}$	0.4263	0.3098	0.0848	0.5412	0.0352	0.4239
$SymHS_{FW}$	0.1456	0.1557	0.0230	0.0504	0.0434	0.1766
$SymDM_{BW}$	0.9888	1.4286	1.2043	2.8133	0.1571	1.3583
$SymDM_{FW}$	0.2422	0.3167	1.0460	0.6865	0.2912	0.9983

The results of the Jacobian analysis are shown in Table 4.4. The Jacobian values of DIR in kVCT and MVCT were not significantly different, with the p-value = 0.7568, 0.1495, and 0.4347 for phantom with rigid changes, phantom with non-rigid changes, and clinical cases, respectively.

Table 4.4 Jacobian analysis compared with different DIR methods between kVCT and MVCT images for phantom with both rigid and non-rigid changes and NPC cases.

DIR methods	Jacobian analysis					
	Phantom (Rigid)		Phantom (Non rigid)		NPC cases	
	kV	MV	kV	MV	kV	MV
$AsyHS_{BW}$	0.9885	0.9726	1.0116	1.0043	1.0037	1.0146
$AsyHS_{FW}$	0.9922	1.0000	0.9905	1.0121	1.0008	1.0452
$AsyDM_{BW}$	0.9956	0.9871	1.0019	0.9922	0.9894	0.9261
$AsyDM_{FW}$	0.9957	1.0078	0.9949	1.0046	0.9962	0.9885
$SymHS_{BW}$	0.9878	0.9737	1.0065	0.9676	1.0045	0.9626
$SymHS_{FW}$	0.9940	1.0262	0.9890	1.0310	0.9956	1.0247
$SymDM_{BW}$	0.9873	0.9360	0.9432	0.9987	1.0079	0.8973
$SymDM_{FW}$	0.9796	0.9924	0.9487	1.0121	0.9801	1.0019

A comparison of DIR accuracy between kVCT and MVCT images revealed that they were not significantly different, based on intensity, volume, and physical characteristics of the deformation field. The DIR in the kVCT images were significantly better than the DIR in the MVCT images in NMI analysis and DSC value only in the rigid volume changes investigation. Different deformation algorithms, transformation frameworks, and sequences of the target domain for generating the mapping direction affect the accuracy

of DIR. Moreover, the accuracy of DIR depends on the ROI as well. There was consistency between the known offset and the unknown offset investigations.

4.1.4 The first three DIR method selection

Regarding the selection of the best three of eight DIR methods to use for dose accumulation, the generic image similarity metric does not exist, but there is a set of metrics that are appropriate for particular applications (Kristy et al .,2013). Intensity-based criterion used to ensure image matching quality, the deformation analysis in terms of ICE and the Jacobian were used to ensure that the transformations were physically plausible. For adaptive radiotherapy application, the main evaluation tools were the dice similarity coefficient (DSC). A DSC value greater than 0.7 is typically selected to indicate good segmentation performance for adaptive radiotherapy application (Kristy *et al*., 2013).

Regarding the DSC analysis, the overlapping volume of the structure which is created by the radiation oncologist and the DIRART deformed for known and unknown offset were evaluated. The Figure 4.14 illustrates the DSC values for the known offset in rigid volume changes and unknown offset for rigid organ changes (spinal cord). The methods with $AsyHS_{BW}$, $AsyHS_{FW}$, $AsyDM_{FW}$, $SymHS_{BW}$, $SymHS_{FW}$ and $SymDM_{FW}$ (no.1, 2, 4, 5, 6 and 8) demonstrated good performance with DSC more than 0.7 for both known and unknown offset.

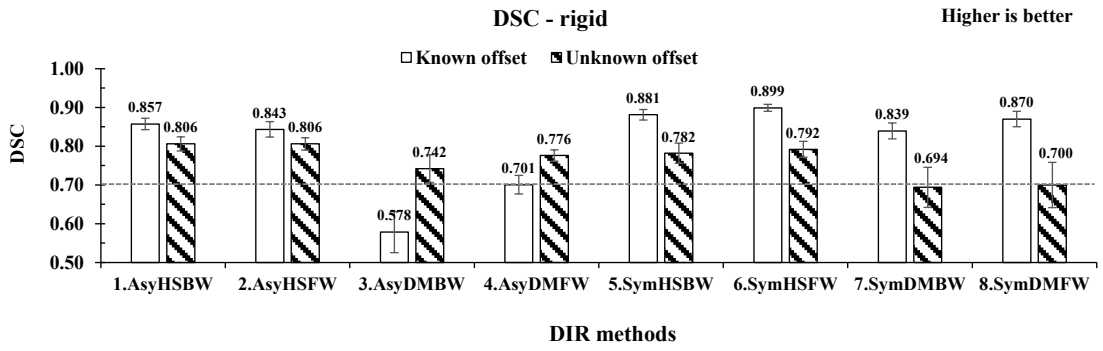

Figure 4.14 The DSC values of the known offset in rigid volume changes and unknown offset for rigid organ change (spinal cord).

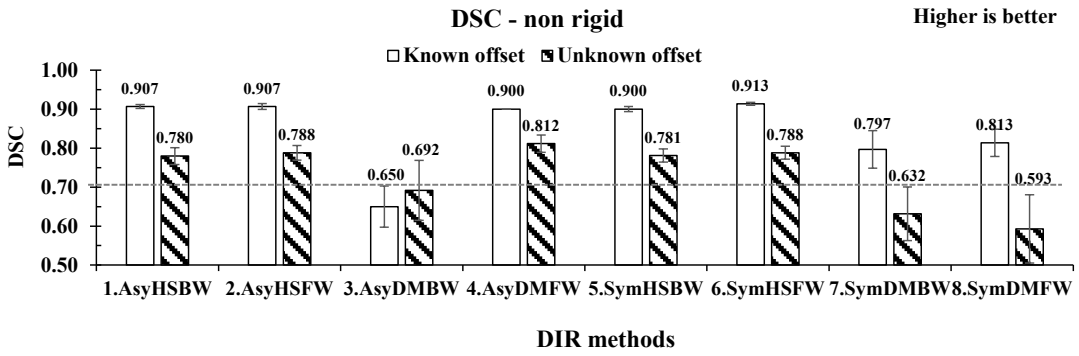

Figure 4.15 The DSC values of the known offset in non-rigid volume changes and unknown offset for non-rigid organ changes.

The DSC values for the non-rigid changes in known offset and unknown offset investigation were demonstrated in Figure 4.15. There were concordant between both investigations, the DIR methods number 1, 2, 4, 5 and 6 also showed better performance with DSC more than 0.7 in non-rigid observed. Moreover, the $AsyDM_{FW}$ (no.4), the mean value of DSC was found to be significantly increased in both known and unknown offset and reached the best performance in unknown offset investigation. Therefore, method number 1, 2, 4, 5, and 6 showed concordance performance in both known and unknown with both rigid and non-rigid changes. When considered in the intensity-based criterion, the methods number 1, 2, 4, 5, and 6 also showed better performance in terms of CC, MSD and NMI. However, the deformation field analysis, the method number 2, 4, and 6 showed the better agreement for deformation vector field analysis, especially in the ICE values. Therefore, the DIR methods with $AsyHS_{FW}$ (no.2), $AsyDM_{FW}$ (no.4) and $SymHS_{FW}$ (no.6) were selected for the accumulated dose estimation in phase II of this study because it can yield the acceptable value in all validation techniques.

4.2 Phase II: Accumulated dose evaluation

As regards the second research objective, the same groups of patients which designed to evaluate the DIR accuracy were also used to evaluate the dosimetric impact of the deformation methods for estimating the weekly dose accumulation on MVCT images. The first three of eight DIR methods was selected to estimate the dose accumulation in this phase of the study

4.2.1 ROIs volume variations

Regarding volume variations during the radiotherapy, the percent ratio to the volume at the initial treatment planning of five NPC patients is illustrated in Figure 4.16. The averages of the five NPC patients for the volume variation in the initial plan were significantly decreased after the treatment in 3 weeks for GTV, with p-value = 0.025, as demonstrated in Figure 4.16 (a), and for CTV, with p-value = 0.020, as demonstrated in Figure 4.16 (b). The volume was observed to decrease by an average of 29.8% (GTV) and 21.0% (CTV) at the end of the treatment course.

As regards the OARs, the right and the left parotid volume variations were significantly different from those of the initial plan after 5 weeks and 4 weeks of treatment, with p-values of 0.017 and 0.026, respectively. The average volume decreased by 40.3% (right) and 43.6% (left) at the end of the treatment.

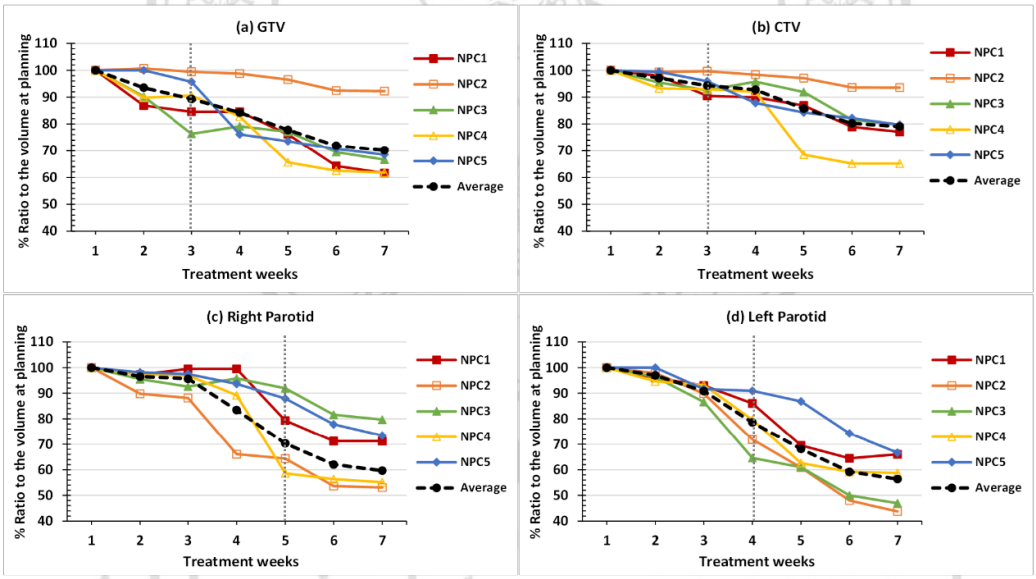

Figure 4.16 Percent ratio to the volume at the initial treatment planning of (a) gross target volume, GTV (b) clinical target volume, CTV (c) right parotid and (d) left parotid glands.

4.2.2 DIR accuracy on weekly MVCT images

As regards the results of DIR accuracy in terms of intensity-based analysis, the correlation coefficient (CC), Figure 4.17 demonstrates the advantages of the

deformable registration when compared with the rigid registration. The rigid registration showed significantly difference from other methods with the one-way ANOVA analysis, p-value = 0.00 with a mean of CC = 0.9363 ± 0.04. Whereas, the three DIR methods presented comparable with a mean of CC values. The $AsyHS_{FW}$ demonstrated slightly better than others with average of mean value CC = 0.9957 ± 0.002.

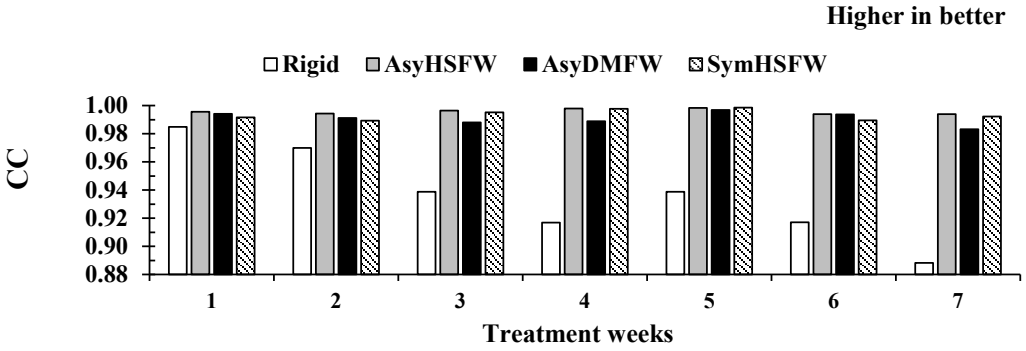

Figure 4.17 Histogram of the correlation coefficient (CC) and the inverse consistency error (ICE) in each treatment week for rigid, asymmetric Horn and Schunck ($AsyHS_{FW}$), asymmetric Demons ($AsyDM_{FW}$) and symmetric Horn and Schunck ($SymHS_{FW}$) with forward mapping deformable image registration (DIR) methods.

There were consistent between the volume-based criterion, DSC, and the deformation field analysis, ICE. Figure 4.18 demonstrates the histogram of the ICE in each treatment week by three DIR methods. The $AsyDM_{FW}$ showed significantly better than other methods by the one-way ANOVA analysis, with p-value = 0.00, with the best performance in terms of ICE values = 0.0058 ± 0.002 mm. The results of ICE were concordant with DSC in all ROIs as in Figure 4.19, the accuracy tended to decrease as the treatment progressed as a result of organs with large-scale deformation causing reduction in the DIR accuracy. The $AsyDM_{FW}$ showed the best agreement with average of mean DSC value = 0.8637 ± 0.03 (GTV), 0.8846 ± 0.04 (CTV), 0.8206 ± 0.04 (right parotid), 0.8503 ± 0.04 (left parotid) and 0.7806 ± 0.02 (spinal cord) for the entire of the treatment.

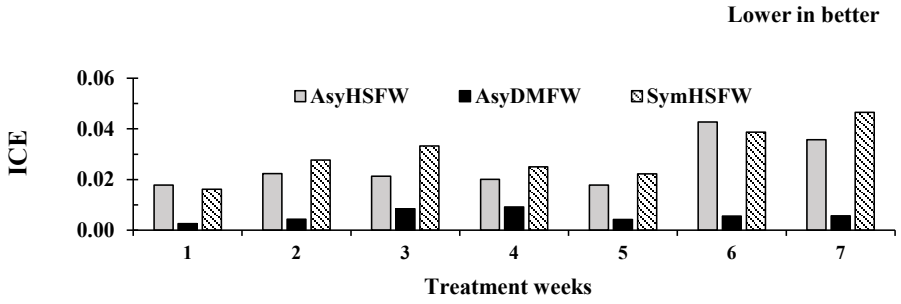

Figure 4.18 Histogram of the correlation coefficient (CC) and the inverse consistency error (ICE) in each treatment week for rigid, asymmetric Horn and Schunck ($AsyHS_{FW}$), asymmetric Demons ($AsyDM_{FW}$) and symmetric Horn and Schunck ($SymHS_{FW}$) with forward mapping deformable image registration (DIR) methods.

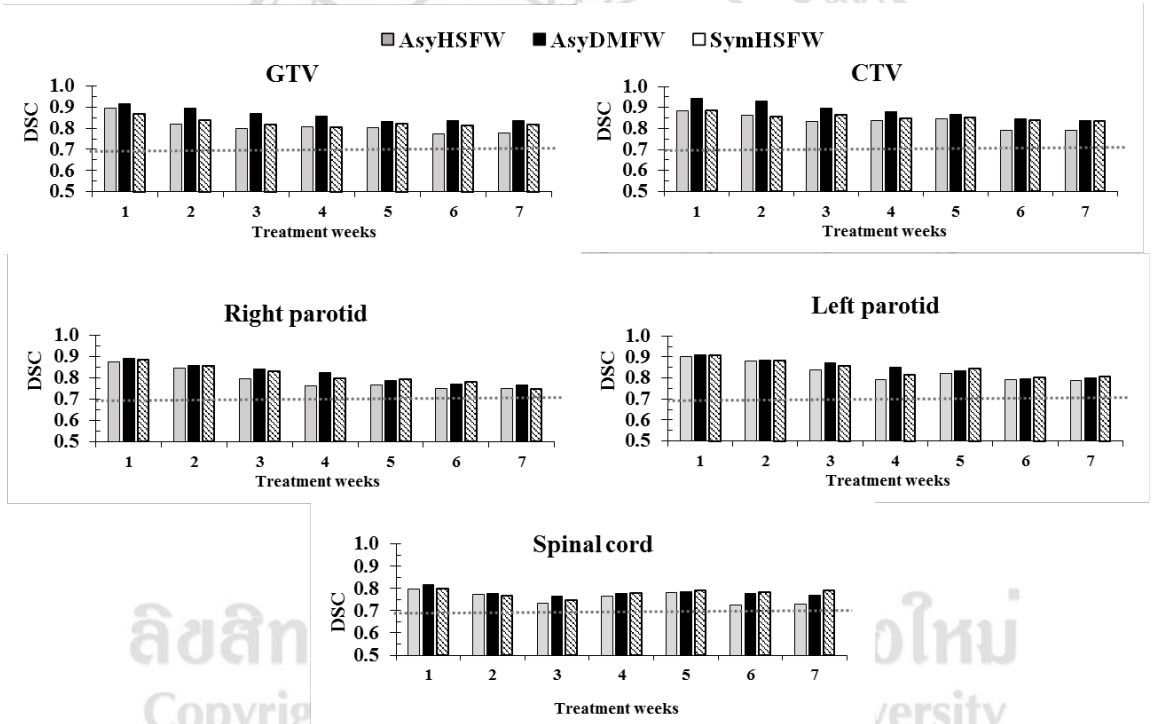

Figure 4.19 Histogram of the dice similarity coefficients (DSC) for all of the target and organ at risk in each treatment week for asymmetric Horn and Schunck ($AsyHS_{FW}$), asymmetric Demons ($AsyDM_{FW}$) and symmetric Horn and Schunck ($SymHS_{FW}$) with forward mapping deformable image registration (DIR) methods.

4.2.3 DIRART and HT planned adaptive software for dose accumulation

To ensure that the weekly dose summation from the DIRART software was accurate, dose accumulation from an independent software, *Planned Adaptive*

software (TomoTherapy Inc., Madison, WI) was used to compare. The same data set of all the reference ROIs on weekly MVCTs defined by the radiation oncologist was transferred to the planned adaptive software and recalculated for the dose accumulation. The comparison of the weekly accumulated doses between DIRART and planned adaptive is illustrated in Figure 4.20.

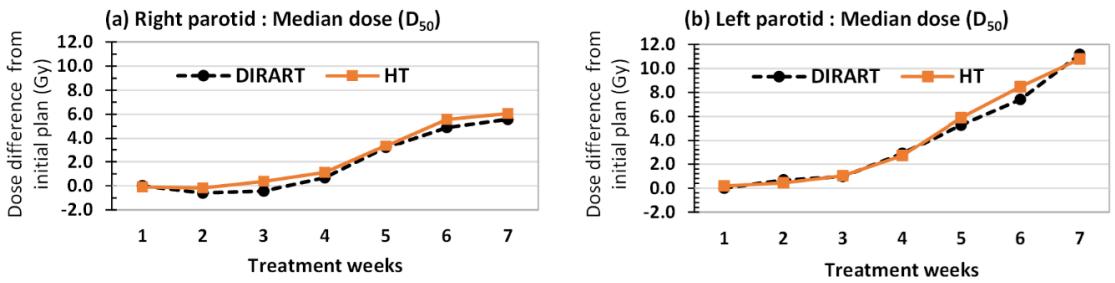

Figure 4.20 Cumulative dose comparison from helical tomotherapy planned adaptive software (HT) and DIRART software in Median dose, D_{50} of (a) Right parotid gland and (b) Left parotid gland.

The variations in the accumulated median parotid doses of DIRART were not significantly different according to the planned adaptive software, with p-value = 0.972 for the right parotid gland, as shown in Figure 4.20 (a), and p-value = 0.958 for the left parotid gland, as shown in Figure 4.20 (b). The consistency in the dose variations between the two independent types of software demonstrates that the dose accumulation of the DIRART software can be applied for dose accumulation studies.

4.2.4 Accumulated dose variation from initial planned dose

As regards the target dose variation, the median GTV and CTV doses received at the end of treatment were slightly different from those in the initial plan. They were 0.11% (range: 0 to 0.29%) lower than the initial planned dose. The median dose variations of the GTV and CTV were significantly different from the initial planned dose after 6 weeks of treatment, with p-value = 0.016. Regarding the minimum and the maximum doses, they are represented by near-minimum dose ($D_{98\%}$) and near-maximum dose ($D_{2\%}$), respectively. As for the $D_{98\%}$, they received slightly higher doses than the initial plan deals, with an average variation less than

0.5% (range: 0.29 to1.6%). However, they received slightly decreased doses of 0.45% (GTV) and 0.28% (CTV) from the initial doses planned for the D_2.

Regarding organ dose variation, the dose differences tended to increase as the treatment progressed. For the bilateral parotid glands, the discrepancy between the delivered and the planned mean doses was found to have increased by 6.8% (range: 2.2 to 10.9%) for the right parotid and by 15.2% (range: -1.7 to 36.3%) for the left parotid. The average mean parotid dose increased in the ranges of 2.24 ± 0.97 Gy (right) and 5.70 ± 4.12 Gy (left) at the end of the treatment. The mean parotid dose variations were significantly different from the initial plan after 6 weeks (right) and 5 weeks (left) of the treatment, with p-value = 0.049 (right) and p-value = 0.010 (left). The spinal cord dose received increased by 6.4% (range: -1.6 to 13.2%) from the initial plan, with the average near-maximum dose increasing in the range of 1.83 ± 1.5 Gy at the end of the treatment.

4.2.5 Impact of DIR methods on weekly dose accumulation

For each patient, the running cumulative doses were calculated using the CERR software through the three deformable image registration methods carried out by the DIRART software. Figure 4.21 demonstrates the 1st DAY MVCT image with original bilateral parotid glands (a) and the MVCT image at fraction 31st with the automatic deformed contour obtained using the $AsyDM_{FW}$ method (b). The initial planned dose distribution on the 1st DAY MVCT image, as illustrated in Figure 4.21 (c), was used for comparison with the accumulated dose distribution at the end of the treatment, as demonstrated in Figure 4.21 (d).

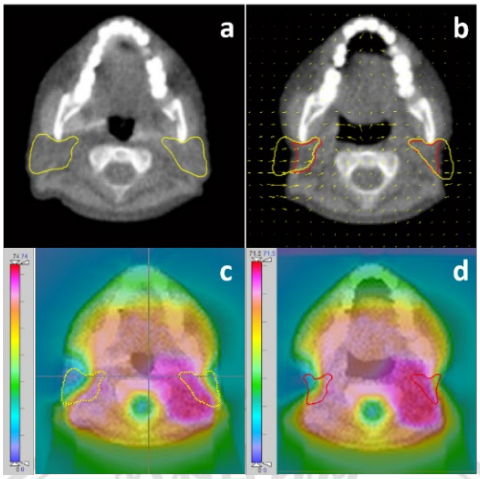

Figure 4.21 The 1stDAY MVCT image with original bilateral parotid glands (a) and the MVCT image at 31st fraction with the automatic deformed contour (b) from $AsyDM_{FW}$ method. The initial plan dose distribution on 1stDAY MVCT image (c) used to compare with the accumulated dose distribution at the end of treatment (d).

The variations in the cumulative doses between the delivered dose and the initial planned dose are illustrated in Figure 4.22 and 4.23.

GTV ($D_{50\%}$): Regarding the Figure 4.22 (a), the weekly GTV dose variation from the initial plan with three DIR methods were illustrates. The average of the median dose (D_{50}) difference for all methods at the end of the treatment was lower than that in the initial plan, with 0.34 Gy (0.5%), 0.04 Gy (0.1%), and 0.30 Gy (0.4%) for the $AsyHS_{FW}$, $AsyDM_{FW}$, and $SymHS_{FW}$ DIR methods, respectively. However, the reference dose of GTV was found to have decreased by 0.11%, with the accumulated GTV dose at 70.12 Gy (range: 69.9 to 70.4 Gy), at the end of treatment.

GTV ($D_{98\%}$, and *$D_{2\%}$):* As regards the near-minimum dose ($D_{98\%}$) and the near-maximum dose ($D_{2\%}$), the $D_{98\%}$ of GTV in three DIR methods were found to be lower than that in the initial plan, as illustrated in Figure 4.22 (b); the average discrepancy of the three DIR methods between the planned dose and the delivered dose was 0.33 Gy (0.5%) at the end of the treatment. However, the reference near-minimum dose was found to have increased by 0.43% of the initial planned dose, with 69.2 Gy (range: 68.7 to 70 Gy). As for the maximum GTV dose consideration,

the three DIR methods of $D_{2\%}$ are presented in Figure 4.22 (c). The average $D_{2\%}$ from the three methods was lower than the initial $D_{2\%}$, with 0.76 Gy (1.1%), at the end of the treatment. The reference $D_{2\%}$ was found to have decreased by 0.45% of the initial planned dose, with 71.5 Gy (range: 70.9 to 72.5 Gy).

CTV ($D_{50\%}$): As regards the median CTV dose, the dose variations tended to be similar to the dose variations of GTV. Figure 4.22 (d) illustrates the difference in the median CTV dose from the initial planned dose. The discrepancy at the end of the treatment was lower than that in the initial planned dose, by 0.34 Gy (0.4%), 0.02 Gy (0%), and 0.26 Gy (0.4%) for $AsyHS_{FW}$, $AsyDM_{FW}$, and $SymHS_{FW}$ DIR methods, respectively. However, the reference median dose was found to have decreased by 0.11%, with 70.12 Gy (range: 69.9 to 70.4 Gy) at the end of the treatment.

CTV ($D_{98\%}$, $D_{2\%}$): the discrepancy between the initial and the delivered dose of the three DIR methods are shown in Figure 4.22 (e). The average of the $D_{98\%}$ variations from the initial $D_{98\%}$ in the three DIR methods was 0.89 Gy (1.2%). Figure 4.22 (f) shows the $D_{2\%}$ of CTV; the average variation from the initial $D_{2\%}$ of the three DIR methods was 0.76 Gy (1.1%).

As regards organ dose accumulation in the three DIR methods, Figure 4.23 illustrates the weekly dose difference from the initial plan in the three DIR methods for the bilateral parotid gland and the spinal cord. Overall, the dose differences tended to increase as the treatment progressed.

Right parotid (D_{mean}): Figure 4.23 (a) shows the mean right parotid dose (D_{mean}) to be higher than the initial planned dose, by 5.38 Gy (16.0%), 3.38 Gy (10.1%), and 4.84 Gy (14.4%) for the $AsyHS_{FW}$, $AsyDM_{FW}$, and $SymHS_{FW}$ methods, respectively. However, the reference mean dose was found to have increased by 2.24 Gy (range: 0.8 to 3.7 Gy), at 6.82%, at the end of the treatment.

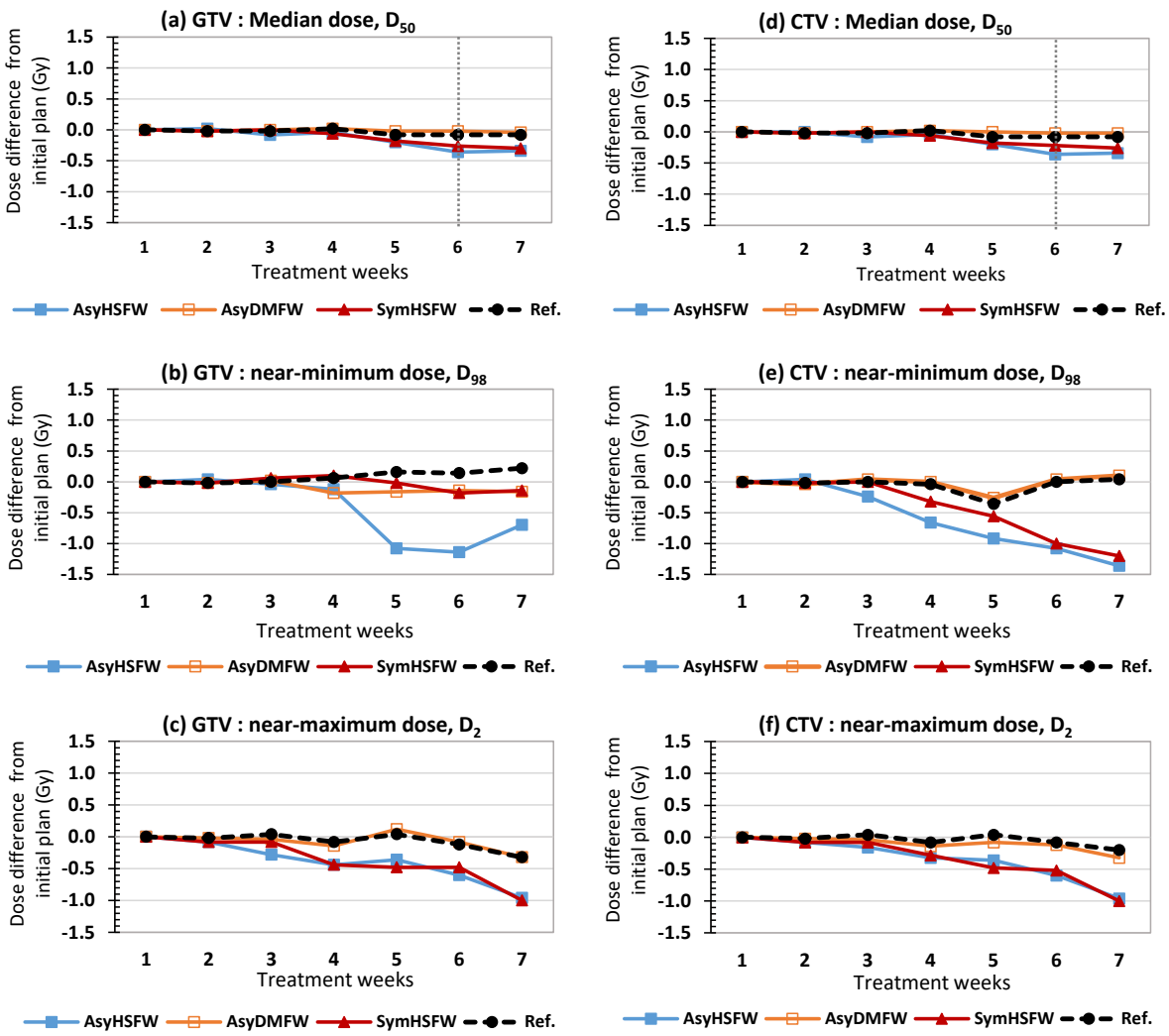

Figure 4.22 Cumulative dose comparison, calculated by the Asymmetric Horn and Schunck ($AsyHS_{FW}$), Asymmetric Demon ($AsyDM_{FW}$) and Symmetric Horn and Schunck ($SymHS_{FW}$) deformable registration methods of gross tumor volume (GTV) for (a) Median dose, $D_{50\%}$ (b) near-minimum dose, $D_{98\%}$ (c) near-maximum dose, $D_{2\%}$ and clinical tumor volume (CTV) for (d) Median dose, $D_{50\%}$ (e) near-minimum dose, $D_{98\%}$ (f) near-maximum dose, $D_{2\%}$. The reference (Ref) accumulated dose was computed by summing the weekly doses corresponding on the weekly MVCTs defined by the radiation oncologist.

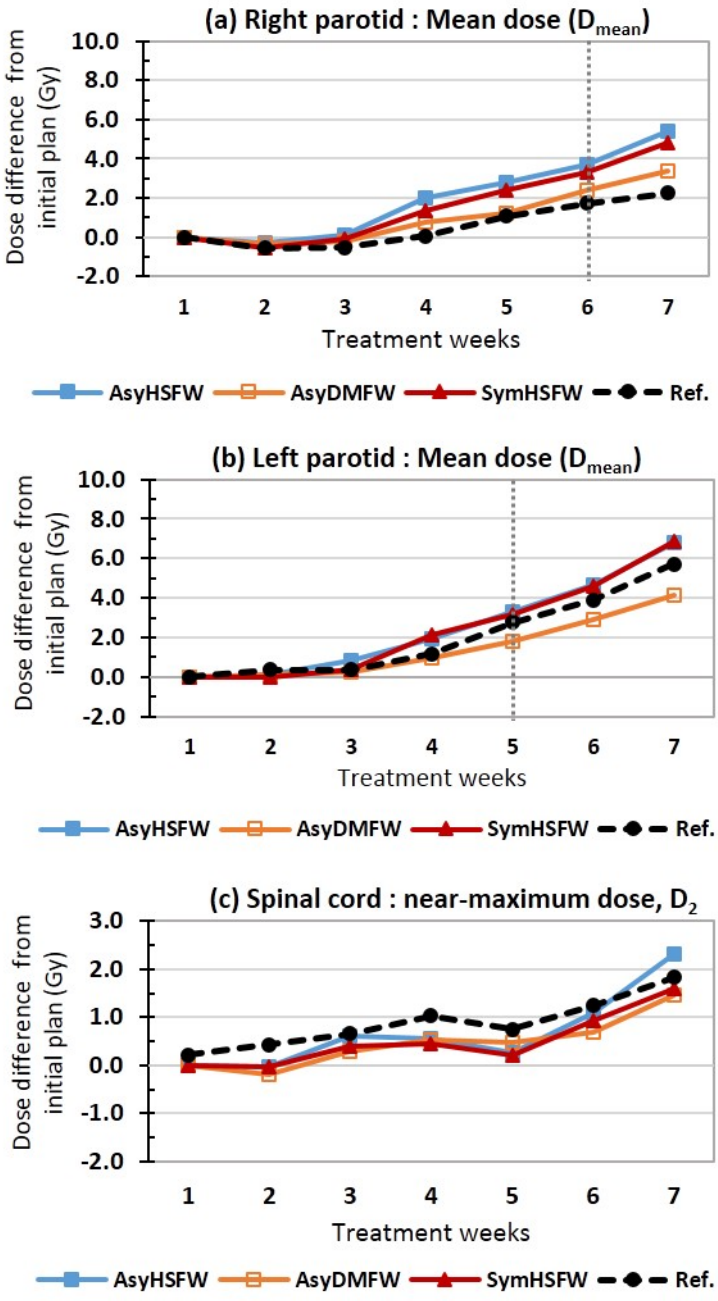

Figure 4.23 Cumulative dose comparison, calculated from the Asymmetric Horn and Schunck ($AsyHS_{FW}$), Asymmetric Demon ($AsyDM_{FW}$) and Symmetric Horn and Schunck ($SymHS_{FW}$) deformable registration methods in Mean dose, D_{mean} of (a) Right parotid gland (b) Left parotid gland and near-maximum dose, $D_{2\%}$ of (c) Spinal cord.

Left parotid (D_{mean}): For the left parotid mean dose, as illustrated in Figure 4.22 (b), these variations were higher than those for the initial planned dose, and

the discrepancy was by 6.88 Gy (18.3%), 4.12 Gy (11.0%), and 6.82 Gy (18.1%) for the $AsyHS_{FW}$, $AsyDM_{FW}$, and $SymHS_{FW}$ DIR methods, respectively. However, the reference mean dose was found to have increased by 5.7 Gy (range: -0.6 to 12.4 Gy), at 15.2% at the end of the treatment.

Spinal cord ($D_{2\%}$): As regards spinal cord weekly dose accumulation, the variations tended to increase in all the three DIR methods, by 2.33 Gy (7.9%), 1.46 Gy (4.9%), and 1.60 Gy (5.4%) for $AsyHS_{FW}$, $AsyDM_{FW}$, and $SymHS_{FW}$, respectively. However, the reference cord dose variation was found to have increased by 1.83 Gy (range: 0.5 to 4.0 Gy), at 6.37% at the end of the treatment.

Table 4.5 The mean uncertainty for estimated the accumulated target and organ dose in each DIR method.

DIR Methods	uncertainty (Gy)			
	GTV	Right parotid	Left parotid	Spinal cord
$AsyHS_{FW}$	0.32	2.86	0.90	0.49
$AsyDM_{FW}$	0.06	1.00	1.48	0.41
$SymHS_{FW}$	0.24	2.12	1.18	0.36
Average	**0.21**	**1.99**	**1.19**	**0.42**

When the uncertainty (difference between the maximum dose and the minimum dose) was considered in the estimation of the accumulated dose, the mean uncertainty for estimated the target and organ dose in each DIR method are shown in Table 4.5. There was consistency between the accuracy of ROIs deformation and discrepancy of dose accumulation.